

# Supernova 1987A: Rotation and a Binary Companion

T.J.B. Collins

Laboratory for Laser Energetics,  
University of Rochester, 250 E. River Rd., Rochester, NY 14623-1299

Adam Frank

Dept. of Physics and Astronomy and C. E. K. Mees Observatory,  
University of Rochester, Rochester, NY 14627-0171

J.E. Bjorkman

Dept. of Physics and Astronomy, Ritter Observatory,  
University of Toledo, Toledo, OH 43606-3390

Mario Livio

Space Science Telescope Institute, 3700 San Martin Dr. Baltimore, MD 21218

Draft September 6, 2018

Received \_\_\_\_\_; accepted \_\_\_\_\_

## ABSTRACT

In this paper we provide a possible link between the structure of the bipolar nebula surrounding SN1987A and the properties of its progenitor star. A Wind Blown Bubble (WBB) scenario is employed, in which a fast, tenuous wind from a Blue Supergiant expands into a slow, dense wind, expelled during an earlier Red Supergiant phase. The bipolar shape develops due to a pole-to-equator density contrast in the slow wind (*i.e.*, the slow wind forms a *slow torus*). We use the Wind Compressed Disk (WCD) model of Bjorkman & Cassinelli (1992) to determine the shape of the slow torus. In the WCD scenario, the shape of the torus is determined by the rotation of the progenitor star. We then use a self-similar semi-analytical method for wind blown bubble evolution to determine the shape of the resulting bipolar nebula.

We find that the union of wind-compressed-disk and bipolar-wind-blown-bubble models allows us to recover the salient properties of SN1987A’s circumstellar nebula. In particular, the size, speed and density of SN1987A’s inner ring are easily reproduced in our calculations. An exploration of parameter space shows that the red supergiant progenitor must have been rotating at  $\gtrsim 0.3$  of its breakup speed. We conclude that the progenitor was most likely spun up by a merger with a binary companion. Using a simple model for the binary merger we find that the companion is likely to have had a mass  $\gtrsim 0.5M_{\odot}$ .

## 1. Introduction

The rings surrounding SN1987A (Burrows *et al.* 1995) are one example of the ubiquitous phenomenon known as a bipolar outflow. These hypersonic, figure-8 shaped nebulae occur in almost all forms of evolved stars, regardless of their mass (*e.g.*, Planetary Nebulae: Manchado *et al.* 1996; Schwartz, Corradi & Melnick 1992; Balick 1987, Luminous Blue Variables: Nota *et al.* 1995; and see Livio 1997 for a review).

Considerable progress has been made in understanding bipolar outflows resulting from interacting stellar winds. Analytical and numerical studies have recovered many of the observed features of these outflows through the *Generalized Wind Blown Bubble* (GWBB) paradigm (Kwok & West 1984; see Frank 1998 for a review). In this scenario, a fast wind from a central source expands into a highly aspherical (*i.e.*, toroidal) environment. The interaction of the wind and its environment produces an expanding bubble bounded by strong shocks. The bubble’s velocity is highest in the direction of lowest density. As a result, the density gradient in the environment (the *slow torus*), establishes a preferred axis for the bipolar lobes. The GWBB paradigm has been successfully applied to all forms of evolved-star bipolar outflows. Models which include the relevant hydrodynamics and microphysics have recovered the global morphology, kinematics and ionization patterns in many planetary nebulae (PNe; Frank & Mellema 1994, Mellema 1996, Dwarkadas, Chevalier & Blondin 1995). Clear correspondences also exist between GWBB models and the shapes and kinematics of Wolf-Rayet (WR) nebulae (Garcia-Segura & MacLow 1993), LBVs like  $\eta$  Carina (Frank, Balick & Davidson 1995) and symbiotic stars like R Aquarii (Henney & Dyson 1992).

The success of the GWBB paradigm opens the possibility of using the properties of a nebula to infer the history of the central star in terms of its mass loss. We note that as of yet no studies have attempted to make an explicit and quantitative link between the properties of the nebula and history of the star. The intense scrutiny applied to SN87A makes it a unique laboratory for studying the connection between bipolar outflows and stellar evolution. Such is the goal of this paper. The recent discovery of a bipolar outflow surrounding Sher 25 (Brander *et al.* 1997), a

star similar to the progenitor of SN87A, also raises the possibility that SN87A is not an isolated object, but defines a new class of bipolar outflows.

When the central ring of SN87A was discovered, it was quickly interpreted as the waist of a bipolar wind-blown bubble (Luo & McCray 1991, Wang & Mazzuli 1992; a structure anticipated by Soker & Livio 1989). In these models the ambient medium was taken to be a toroidal wind deposited by SN87A’s progenitor in its Red Supergiant (RSG) stage. The bubble was subsequently inflated by a fast wind from the star’s penultimate incarnation as a Blue Supergiant (BSG). The first numerical simulations of this process were carried out by Blondin & Lundqvist (1993: BL93) who used an *ad hoc* function to determine the asphericity of the slow RSG wind. BL93 were quite successful in demonstrating the feasibility of the GWBB paradigm for SN87A. However, the observed low expansion speed of the central ring ( $v_{\varpi} \approx 8 \text{ km s}^{-1}$ , Meaburn *et al.* 1995) presented a problem. To create a model with the correct kinematics, BL93 were forced to adopt very low values of both the RSG and BSG wind velocities. In particular, their value of the RSG wind speed,  $v_a \sim 5 \text{ km s}^{-1}$ , seemed particularly anomalous. Canonical values for Red Giant winds are comparable to 20 km/s (Habing 1996). BL93 were also forced to take an equator-to-pole density contrast of  $p = \rho_e/\rho_p = 20$ , which, at the time, seemed large. The size of  $p$  was one reason cited by McCray & Lin 1992 in their arguments that the ambient density distribution represented a remnant protostellar disk rather than a stellar wind (although more recently the protostellar disk idea has been abandoned, McCray, private communication). Martin and Arnett (1994, MA95) carried out GWBB simulations similar to Blondin & Lundqvist. Using a different *ad hoc* function to control the density asymmetry of the RSG wind, MA95 confirmed Blondin & Lundqvist’s results, including the need for low RSG wind speeds,  $v_a < 10 \text{ km/s}$ . We note that both BL93 and MA95 assumed that the the RSG wind speed was isotropic.

The discovery of additional upper and lower rings of SN87A both confirmed and confused the image of SN87A’s nebula as a bipolar outflow. While a number of different models for the the formation of these outer rings have been proposed (*e.g.*, Burrows *et al.* , 1995; MA95; Podsiadlowski, Fabian & Stevens, 1991; Lloyd, O’Brian & Kahn, 1995; Meyer, 1997), there does

not yet exist a generally accepted model.

In spite of the difficulties associated with the upper and lower rings, the consensus appears to be that the GWBB model has proven effective for SN87A (Crotts 1998). Its success has allowed researchers to pose basic questions about the progenitor. In particular, the need for an aspherical RSG wind has led a number of authors to posit the existence of a binary companion for the progenitor of SN87A. Soker (1998) and Livio (1998) have argued that binary companions are required to produce slow toroids in PNe; similar arguments hold for SN87A (Livio 1997). Using considerations from stellar evolution theory, along with the need for a high equator to pole contrast, Podsiadlowski (1992) also argued that SN87A was a binary system. He calculated a likely companion mass of 3 to 6  $M_{\odot}$  with the progenitor/primary of 16  $M_{\odot}$ . Podsiadlowski concluded that the two stars merged before the supernova, which is consistent with the lack of observational evidence for a companion in the post-supernova epoch (*e.g.*, Crotts, Kunkle & Heathcote, 1995).

In this paper, we take up the challenge posed by previous models: whereas previous investigations have used an *ad hoc* description of the aspherical RSG, we will link the shape of this slow torus to the properties of the star itself. Currently, the best generic scenarios for developing asphericity in a slow wind are Common Envelope interactions in binary stars (Livio & Soker 1988) and the Wind Compressed Disk (WCD) model of Bjorkman & Cassinelli (1993). In the Common Envelope model, a slow, dense wind which has higher mass loss in the orbital plane of the binary system is ejected by the primary. While this process has been shown to be effective (Terman *et al.*, 1995; Rasio & Livio, 1996), calculations of the wind shape require numerical models which must span a large range in both length and time scales. Thus, there is no simple means for linking initial states of the binary with the shape of the ejected slow torus. The WCD model, which was developed for excretion disks surrounding B[e] stars, relies on the equatorial focusing of wind streamlines from rapidly rotating stars. The advantage of the WCD mechanism is its relatively simple formalism, which relates the properties of a single star (mass, temperature, mass loss rate, rotation rate) with the properties of the slow torus. The WCD mechanism has been adapted to Red Giant stars (Ignace, Bjorkman & Cassinelli, 1996) and has already been used to produce slow

tori in LBV and PNe bipolar outflow simulations (Garcia-Segura *et al.* , 1997a; Garcia-Segura *et al.* , 1997b).

The goal of the present paper is to utilize the WCD and GWBB formalisms to establish the efficacy of the the combined model for SN87A. We then work backwards to bracket the properties of the progenitor based on the comparison of models with observations. In what follows, we describe self-similar models of the nebula surrounding SN87A, which employ a WCD model to determine the properties of the RSG wind. Our self-similar model is based on the work of Giuliani (1982) and Dwarkadas, Chevalier & Blondin (1995; hereafter DCB95). We use observations of the rings surrounding SN87A to constrain the parameters of the system, and to explore the implications for the rotation rate of the progenitor. In §2 we describe the WBB and WCD models. In §3 the results of the models and a comparison with observations are presented, as well as a “fiducial,” or “best-fit” model for the nebula. In §4 the implications of these results for the progenitor are explored. Lastly, in §5 we discuss our results.

## 2. Theory

When a stellar wind “turns on,” it expands ballistically until enough ambient material is swept up for significant momentum to be exchanged between the wind and the ambient medium (Koo & McKee 1992). A triplet of hydrodynamic discontinuities then form, defining an “interaction region” bounded internally (externally) by undisturbed wind (ambient) gas. The outer boundary is an outward-facing shock. It accelerates, compresses, and heats the ambient material as it propagates. We refer to this as the *ambient shock*, and denote its position as  $R$ . The inner boundary is defined by an inward-facing shock which decelerates, compresses and heats the stellar wind. We refer to this feature as the *wind shock*. Its position is  $R_{ws}$ . A *contact discontinuity* (CD),  $R_{cd}$ , separates the shocked wind and shocked ambient material. In the 1 dimensional (1-D) bubble these discontinuities form a sequence in radius:  $R_{ws} < R_{cd} < R$ .

The compressed gas behind either or both shocks emits strongly in optical, UV and IR

wavelengths producing a bright shell which defines the observable “bubble.” In SN87A, compressed material at the equator defines the central ring. The dynamics of the bubble and its emission characteristics are defined by the efficiency of post-shock shock cooling. Behind each shock we can define a cooling time-scale  $t_c = E_t/\dot{E}_t$ , where  $E_t$  is the thermal energy density of the gas. Radiative cooling can be expressed in terms of a cooling function:  $\dot{E}_t = C(T) = n^2\Lambda(T)$ , where  $n$  is the number density of the gas,  $T$  its temperature, and the function  $\Lambda(T)$  is a sum over many radiative processes emitting at a variety of wavelengths. The bubble has cooling and dynamical time scales defined as

$$t_c = \frac{3kT}{2n\Lambda(T)} \quad (1)$$

$$t_d = \frac{R}{V}, \quad (2)$$

where  $V$  is the speed of the ambient shock,  $k$  is Boltzmann’s constant, and we have assumed (as we shall throughout this paper) that  $\gamma = 5/3$ . Comparison of  $t_c$  and  $t_d$  separates WBBs into two classes: Radiative (referred to as *momentum conserving*) and Adiabatic (or *energy conserving*).

In what follows we assume that the BSG wind speed is large enough that the shocked wind is extremely hot, and cools inefficiently *i.e.*,  $t_c \gg t_d$ . In this case the wind shock is adiabatic and hot shocked wind material fills the expanding bipolar bubble, causing expansion through thermal pressure, so that a *hot bubble* forms. We also assume that the shocked ambient material cools efficiently, so that  $R_{cd} \approx R$ . DCB95 showed that for thermal-pressure-supported, or *energy conserving* bubbles, the expansion is self-similar for a significant portion of its evolution. The resulting, simplified equations may then be solved without resorting to time-dependent hydrodynamical calculations.

The parameters of this wind-blown bubble (WBB) model include the description of the BSG and RSG winds. Specifically, the wind speeds and mass loss rates of the two winds must be supplied, as well as the dependence of the wind speeds on the polar angle  $\theta$ , given by the asymmetry functions  $f(\theta)$  for the RSG wind density, and  $g(\theta)$  for the RSG wind speed, defined by

$$g(\theta) = \lim_{r \rightarrow \infty} v_r/v_a, \quad (3)$$

$$f(\theta) = \lim_{r \rightarrow \infty} 4\pi r^2 v_a \rho / \dot{M}_a. \quad (4)$$

In previous models of SN87A, these asymmetry functions have been determined *ad hoc* (e.g., Luo & McCray, 1991; BL93). Here we assume that the balance of wind driving and centrifugal forces focuses the RSG wind toward the equatorial plane, creating a *wind-compressed disk* (WCD: Bjorkman and Cassinelli, 1993). A solution of the WCD equations yields  $f(\theta)$  and  $g(\theta)$ . We note again that all previous studies assumed an isotropic RSG wind velocity, so that  $g(\theta)$  is constant, whereas the WCD model naturally proscribes a wind asphericity. In the following sections we describe the models used for the wind blown bubble and the environment.

## 2.1. Wind-Blown Bubble Model

The general equations describing the evolution of a thin shell have been derived by Giuliani (1982). In the DCB95 model, these equations are applied to a shell of swept-up, shocked Asymptotic Giant Branch star wind material which forms the bright optical regions of Planetary Nebulae. Here we apply the model to the swept-up RSG gas. It is assumed that the width of the shell is much smaller than its radius, and that magnetic fields may be neglected. The velocity and density are averaged over the width of the shell. We briefly sketch the derivation of the equations here; the complete derivation may be found in DCB95.

The continuity equation for the shell is given by

$$\frac{\partial \sigma}{\partial t} = -\rho_o(v_{\perp o} - u_{\perp}) + \rho_i(v_{\perp i} - u_{\perp}) - \sigma \frac{\partial \ln A}{\partial t} - \frac{1}{A} \frac{\partial}{\partial \theta} (R \sin \theta \sigma (v_{\parallel} - u_{\parallel})). \quad (5)$$

Here  $\sigma$  is the internal column density of the shell,  $\rho$  is the volume density,  $\mathbf{v}$  is the wind velocity, and  $\mathbf{u}$  is the shell velocity. The independent variables are the spherical radius  $r$ , the spherical polar angle  $\theta$ , and the time  $t$ , and  $R(\theta, t)$  is the radius of the shell. The quantities inside the bubble are labeled with the subscript “o”, while those outside the bubble bear the subscript “i,” and quantities which are averaged over the width of the shell have no subscript. The velocity vectors have been decomposed into components perpendicular (e.g.  $u_{\perp}$ ) and parallel (e.g.  $u_{\parallel}$ ) to

the shell. The quantity  $A$ , used for simplicity of notation, is defined by

$$A \equiv \left( \frac{r^2 \sin \theta}{\cos \xi} \right)_R, \quad (6)$$

where  $\xi$  is the angle between the radius vector and the local normal to the shell surface. The defining equation for  $\xi$  is

$$\tan \xi \equiv -\frac{1}{R} \frac{\partial R}{\partial \theta}. \quad (7)$$

The first two terms on the right-hand side (rhs) of equation (6) represent the flux of mass through the inner and outer surfaces of the shell. The third term represents the change in surface density due to the change in surface area of the bubble, while the final term accounts for flow within the shell.

The perpendicular and parallel components, respectively, of the momentum equation are given by

$$\begin{aligned} \sigma \left( \frac{\partial v_{\perp}}{\partial t} - v_{\parallel} \frac{\partial \xi}{\partial t} \right) &= -[\rho_o(v_{\perp o} - u_{\perp})(v_{\perp o} - v_{\perp})] \\ &\quad + [\rho_i(v_{\perp i} - u_{\perp})(v_{\perp i} - v_{\perp})] + P_i \\ &\quad - (v_{\parallel} - u_{\parallel}) \frac{\sigma \cos \xi}{R} \left[ \frac{\partial v_{\perp}}{\partial \theta} - v_{\parallel} \left( 1 + \frac{\partial \xi}{\partial \theta} \right) \right], \end{aligned} \quad (8)$$

and

$$\begin{aligned} \sigma \left( \frac{\partial v_{\parallel}}{\partial t} - v_{\perp} \frac{\partial \xi}{\partial t} \right) &= -[\rho_o(v_{\perp o} - u_{\perp})(v_{\parallel o} - v_{\parallel})] \\ &\quad + [\rho_i(v_{\perp i} - u_{\perp})(v_{\parallel i} - v_{\parallel})] \\ &\quad - (v_{\parallel} - u_{\parallel}) \frac{\sigma \cos \xi}{R} \left[ \frac{\partial v_{\parallel}}{\partial \theta} + v_{\perp} \left( 1 + \frac{\partial \xi}{\partial \theta} \right) \right], \end{aligned} \quad (9)$$

where  $P_i$  is the thermal pressure causing bubble expansion, and we have assumed that  $P_i \gg P_o$ . In equations (8) and (9), the first two terms on the rhs represent the ram pressure balance. In equation (8) the third term represents the thermal pressure. The derivatives of  $v_{\parallel}$  and  $v_{\perp}$  with respect to  $\theta$  in the final terms of equations (7) and (8) account for the ram pressure balance within the shell, and the term proportional to  $(1 + \partial \xi / \partial \theta)$  is due to the centrifugal force.

The order of these equations may be reduced if one assumes that the flow is self-similar – *i.e.*, that the expansion velocity is proportional to the spherical radius  $r$ . With this assumption, the

radius  $R$  may be written in terms of a self-similar radius  $L$ , using the expansion velocity at the pole,  $v_p$ :  $R(\theta, t) = v_p t L(\theta)$ . For a RSG wind with constant mass flux  $\dot{M}_a$  and radial velocity  $v_a$ , the density outside the bubble may be written

$$\rho_o = \frac{\dot{M}_a f(\theta)}{4\pi v_a R^2}, \quad (10)$$

where  $f(\theta)$  is the asymmetry function, which is identically one for an isotropic wind. The self-similar surface density  $S(\theta)$  is defined by

$$\sigma = \frac{\dot{M}_a S(\theta)}{4\pi v_a v_p t}. \quad (11)$$

The parallel component of the gas velocity within the shell is given by

$$v_{\parallel} = v_p U(\theta). \quad (12)$$

The parallel and perpendicular components of the shell velocity are defined by

$$u_{\parallel} = -\frac{\partial R}{\partial t} \sin \xi, \quad u_{\perp} = \frac{\partial R}{\partial t} \cos \xi, \quad (13)$$

so that

$$u_{\parallel} = -v_p \sin \xi L(\theta), \quad u_{\perp} = v_p \cos \xi L(\theta). \quad (14)$$

Because the BSG wind undergoes a strong shock,  $u_{\perp} \approx v_{\perp}$ . The velocities outside the bubble are

$$v_{\perp o} = v_a g(\theta) \cos \xi, \quad v_{\parallel o} = -v_a g(\theta) \sin \xi, \quad (15)$$

where  $g(\theta)$  is the asymmetry of the RSG wind velocity. Because the RSG wind is assumed to have a constant mass flux,  $f(\theta) = 1/g(\theta)$ . We assume without loss of generality that  $f(0) = 1$ , and that  $L(0) = 1$ . Finally, the pressure inside the bubble is proportional to  $\rho v^2$ . Given that the mass flux is constant,  $\rho \sim r^{-2}$ . Since  $v \sim r/t$ , we expect  $P_i \sim t^{-2}$ . Thus, we let  $P_i = F/t^2$ , where  $F$  is a constant.

With these substitutions, equations (5) and (7)-(9) become

$$L' = -L \tan \xi, \quad (16)$$

$$\begin{aligned} \xi' &= \frac{L}{S}(U + L \sin \xi)^{-2} \left[ f(\theta) \cos \xi \right. \\ &\quad \left. \times \left( \frac{\lambda_v}{L} - 1 \right)^2 - \sec \xi (\lambda - 1)^2 \right] - 1, \end{aligned} \quad (17)$$

$$U' = \frac{f(\theta)}{S} \left( \frac{\lambda_v}{L} - 1 \right) \left( \frac{U + \lambda_v \sin \xi}{U + L \sin \xi} \right) - L \cos \xi (1 + \xi'), \quad (18)$$

$$\begin{aligned} S' &= S(\tan \xi - \cot \theta) - f(\theta)(U + L \sin \xi)^{-2} \\ &\quad \times \left( \frac{\lambda_v}{L} - 1 \right) (2U + (L + \lambda_v) \sin \xi), \end{aligned} \quad (19)$$

where we have defined  $\lambda \equiv v_a/v_p$ , and  $\lambda_v \equiv \lambda g(\theta)$ .

At the poles there is no flow within the shell, so that  $\xi(0) = U(0) = 0$ . In the limit  $\theta \rightarrow 0$ , the self-similar form of the perpendicular component of the momentum equation (8) yields the equation

$$F = \frac{\dot{M}}{4\pi v_a} (\lambda - 1)^2. \quad (20)$$

This has been used to eliminate  $F$  in equation (15).

The value of  $v_p$  is determined using the equation for bubble energy conservation. The rate of change of internal energy  $E$  is given by the work done by the fast wind,  $l$ , minus the work done to expand the bubble,  $dW/dt$ :

$$\frac{dE}{dt} = l - \frac{dW}{dt}. \quad (21)$$

As is shown in DCB95, this yields the constraint on  $v_p$  of

$$\chi(v_a - v_p) + v_p^{-1/2} \left( \frac{v_f^2 v_a \dot{M}_f}{3\dot{M}_a} \right)^{1/2} = 0, \quad (22)$$

where  $\dot{M}_f$  is the BSG mass loss rate, and  $\chi$  is the ratio of the volume of the bubble to the volume of a sphere with the same polar radius.

The system of equations of solved as follows: A value of  $\lambda$  is assumed. Equations (16)-(19) are then solved numerically to determine the self-similar functions  $L(\theta)$ ,  $S(\theta)$ ,  $U(\theta)$  and  $\xi(\theta)$ . Given  $L(\theta)$  it is possible to calculate numerically  $\chi$ . Equation (22) then yields a new value of  $v_p$ , and thus a new value of  $\lambda$ . Iteration of this procedure may be used to find self-consistent energy-conserving models of the nebula surrounding SN87A.

The four variables  $v_a$ ,  $v_f$ ,  $\dot{M}_f$  and  $\dot{M}_a$  are parameters of the system which are varied to match observations of SN87A. The RSG wind density asymmetry function  $f(\theta)$  is determined using the wind-compressed disk model, described in §2.2, and the velocity asymmetry function  $g(\theta)$  is, as mentioned above, given by its inverse.

Finally, we note that an implementation of the fifth-order Runge-Kutta algorithm was used to solve the WBB equations (16)-(19). A Newton’s method was used to solve the additional constraint of equation (22).

## 2.2. Wind-Compressed Disk Model

The Wind-Compressed Disk Model (Bjorkman & Cassinelli 1993, hereafter BC) was developed to determine the structure of a rotating stellar wind. Their model applies whenever the external forces driving the wind are central (*i.e.*, radial) forces. BC found that, in the supersonic portion of the flow, the wind streamlines originating at high latitudes converge toward the equator. The reason for this behavior may be understood as a simple consequence of orbital dynamics. As the fluid leaves the surface of the star, it tends to orbit around the star until it is accelerated radially outward. If the initial outward acceleration is small compared to the rotation rate of the star, then the material orbits far enough around the star that it crosses the equator, where it meets material from the opposite hemisphere of the star. Since the flow velocities perpendicular to equator are supersonic, a pair of shocks form above and below the equator, and the shock compression of the material entering the equatorial region creates a dense disk. Thus we see that whether or not a disk forms depends on the rotation rate of the star,  $\Omega = V_{\text{rot}}/V_{\text{crit}} = \Omega_*/\Omega_K$ , where  $V_{\text{rot}}$  and  $V_{\text{crit}}$  are the rotation and break-up speeds, and  $\Omega_*$  and  $\Omega_K$  are the stellar and Keplerian rotation rates. If the star rotates faster than a threshold value,  $\Omega > \Omega_{\text{th}}$ , a dense, shock-compressed disk forms, with  $p \sim 100$ . Otherwise, there is only a mild density compression in the equator (typically  $p < 3-10$ ). BC originally applied this model to investigate if the disks around Be stars could be produced by the WCD mechanism. The WCD model was later applied to several other classes of stars, including AGB stars, by Ignace, Cassinelli, & Bjorkman (1996, hereafter ICB).

To model the RSG wind, we follow ICB to obtain the flow velocity and density of the wind. ICB assume that the wind velocity of AGB stars can be described by the usual  $\beta$ -law,

$$v_r(r, \theta) = v_0 + [v_\infty(\theta_0) - v_0] (1 - R_*/r)^\beta, \quad (23)$$

where the initial velocity  $v_0$  equals the sound speed, and  $v_\infty$  is the wind terminal speed. The value of the velocity law exponent,  $\beta$ , determines the acceleration of the wind. ICB assume that the winds of AGB stars are slowly accelerating, so they adopt  $\beta = 3$  in their model.

The wind density is determined by the continuity equation, which yields

$$\rho(r, \theta) = \frac{\dot{M}(\theta_0)}{4\pi r^2 v_r (d\mu/d\mu_0)}, \quad (24)$$

where  $\mu = \cos \theta$ ,  $\mu_0 = \cos \theta_0$ , and  $\theta_0$  is the initial co-latitude (at the stellar surface) of the streamline passing through the point  $(r, \theta)$ . Note that the factor  $(d\mu/d\mu_0)$ , given by equation (B3) of ICB, is the solid angle of the streamtube; this change in cross-sectional area produces the equatorial wind compression and is primarily responsible for the increased density near the equator.

To evaluate the density, we must first determine  $\theta_0$  for the given location  $(r, \theta)$  by solving numerically equation (B2) of ICB. However for our wind-blown bubble model, we are only interested in distances that are quite far away from the star. In the limit  $r \rightarrow \infty$ , equation (A6) of ICB for the azimuthal deflection of the streamline becomes

$$\phi'_{\max}(\theta_0) = \frac{V_{\text{rot}} \sin \theta_0}{\beta v_0} \left( \frac{v_0}{v_\infty(\theta_0) - v_0} \right)^{1/\beta} B_{y_{\max}(\theta_0)} \left( \frac{1}{\beta}, 1 - \frac{1}{\beta} \right), \quad (25)$$

where  $B$  is the incomplete gamma function with the argument  $y_{\max}(\theta_0) = 1 - v_0/v_\infty(\theta_0)$ . In the large- $r$  limit,  $\theta_0$  is given by the solution to the equation

$$\cos \theta_0 \cos \phi'_{\max}(\theta_0) = \cos \theta. \quad (26)$$

With this value for  $\theta_0$ , we then evaluate the wind compression factor  $(d\mu/d\mu_0)$ , given by equation (B3) of ICB, as well as the streamline mass loss rate and terminal speed, which are given by

$$\dot{M}(\theta_0) = \dot{M}_a (1 - \Omega \sin \theta_0)^\xi, \quad (27)$$

$$v_\infty(\theta_0) = v_a (1 - \Omega \sin \theta_0)^\gamma, \quad (28)$$

with  $\gamma = 0.35$  and  $\xi = -0.43$  (see BC).

Substituting equations (24), (27), and (28) into equation (3) and (4), we find the wind asymmetry functions

$$g(\theta) = (1 - \Omega \sin \theta_0)^\gamma, \quad (29)$$

$$f(\theta) = (1 - \Omega \sin \theta_0)^{\xi - \gamma} (d\mu/d\mu_0)^{-1}. \quad (30)$$

These equations are valid for the wind. However, if the stellar rotation rate is above the disk formation threshold ( $\Omega > \Omega_{\text{th}}$ ), then we need the disk properties as well. Unfortunately, the WCD model *per se* cannot determine the disk density and velocities, so we make a simple estimate based on the numerical hydrodynamics simulations by Owocki, Cranmer & Blondin (1994). They found that the disk has an opening angle  $\Delta\theta_d \approx 3^\circ$ , which agrees with observations of Be stars (Wood, Bjorkman & Bjorkman 1997), and that the disk terminal speed  $v_d \sim 0.2\text{--}0.3v_a$ . However based on observations of the disks around Be and B[e] stars (Waters *et al.* 1988, Zickgraf *et al.* 1996), we adopt a slightly lower value  $v_d = 0.1v_a$ . In addition to the geometry and flow speeds, Owocki *et al.* found that there is a stagnation point in the disk. Interior to the stagnation point, the disk material falls back onto the star, while exterior to the stagnation point the disk material flows outward. At low rotation rates, this recirculation is not dominant, so for simplicity we assume that all the wind material entering the disk flows outward. Using the continuity equation, the disk density may be estimated by

$$\rho_d = \frac{\dot{M}_d}{2\pi r^2 \sin \Delta\theta_d v_d}. \quad (31)$$

The mass loss rate entering the disk,

$$\dot{M}_d = \frac{1}{2} \int_0^{\mu_0^d} \dot{M}(\theta_0) d\mu_0, \quad (32)$$

is determined by  $\mu_0^d = \cos \theta_0^d$ , the minimum co-latitude of all streamlines that enter the disk (see Fig. 10 of BC), which is given by the solution to

$$\phi'_{\text{max}}(\theta_0^d) = \pi/2. \quad (33)$$

Using the disk terminal speed,  $0.1v_a$ , and equation (31), we find that the velocity and density asymmetry functions for the disk are

$$g_d = 0.1, \tag{34}$$

$$f_d = \frac{\int_0^{\mu_0^d} (1 - \Omega \sin \theta_0)^\xi d\mu_0}{g_d \sin \Delta\theta_d}. \tag{35}$$

These equations are to be used only when  $\Omega > \Omega_{\text{th}}$  and  $|\theta - \pi/2| < \Delta\theta_d$ ; otherwise, one should use equations (29) and (30).

### 3. Results

As was discussed in §1, the accepted WBB model for SN87A treats the inner ring as the “waist” of the bipolar outflow and assumes that the outer rings lie somewhere on the surface of the lobes or represent lobe edges. In what follows we do not attempt to explain the outer rings, and primarily use the inner ring to constrain the parameters of our models.

We use a number of observed features of SN87A for comparison with the models: The radius of the inner ring,  $\varpi \sim 6.3 \times 10^{17}$  cm, sets the length-scale of our solutions. The density of the inner ring has been found to be at least  $\sim (1 - 2) \times 10^3 \text{ cm}^{-3}$  (Lundqvist & Sonneborn, 1997). Based on optical images, the width of the inner ring,  $\delta r$ , is approximately one tenth of its radius. We use this to convert from column density to volume density:  $\rho_\varpi = \sigma/\delta r$ . The radial velocity of the inner ring is  $v_\varpi \approx 8.3 \text{ km s}^{-1}$  (Meaburn *et al.* 1995). The quantities  $v_\varpi$  and  $\rho_\varpi$  are the primary observations used to constrain the parameters of our models. We note that the polar expansion velocity may be given in terms of the velocity asymmetry function  $g(\theta)$  as  $v_p = v_\varpi f(\pi/2)$ . In addition to  $v_\varpi$  and  $\rho_\varpi$ , we have calculated the ratio of the cylindrical radius of the lobes at their widest points to the radius of the inner ring (which we denote  $R'_o$ ). This is compared with the ratio of the cylindrical radius of the outer rings to that of the inner rings (which we denote  $R_o$ ). The observed value of  $R_o$  is  $\sim 2$ .

### 3.1. Fiducial Models

As described in §2.2, the angular dependence of the RSG wind depends on the ratio  $\Omega$  of the progenitor’s rotation rate to the breakup rotation rate. The equator-to-pole density contrast  $p$  of the RSG wind is therefore proportional to  $\Omega$ . In what follows, we assume that the RSG has a radius of  $740 R_{\odot}$ , a mass of  $20 M_{\odot}$ , and an effective temperature of  $3300 \text{ K}$ . Given these values, the WCD model shows that when  $\Omega \sim 0.3$ , the equator-to-pole density contrast becomes significant,  $p \sim 25$ , even if a shock-bounded “disk” does not form. For  $\Omega \gtrsim 0.3$ , a thin excretion disk forms with a very high density contrast of  $p \gtrsim 700$ . Upon driving a BSG wind into these environments we find we can produce a bipolar wind-blown bubble consistent with the nebula around SN87A. In particular, we can recover the observed properties of the inner ring with two models, one with and one without a disk. The shape, expansion velocity and surface densities of these models are shown in Figs. 1, 2, and their density asymmetry functions  $f(\theta)$  are shown in Fig. 3. The initial parameters and the ring properties for the two models are given in Table 1. In both cases the expansion speed of the ring is equal to  $\sim 8.3 \text{ km s}^{-1}$ . (We have also created a model with a ring expansion speed of  $\sim 10 \text{ km s}^{-1}$ , in accordance with the observations of Crotts *et al.*, 1995, and find that it requires, for the model with the WCD, an  $\Omega$  lower by 0.02; This does not significantly affect the results given by the Binary Merger Model of §4.) The ring density is within a factor of two of observed estimates (Table 1).

It is important to note that we can produce successful models without resorting to anomalously low values for the speed of the RSG wind at the poles. As was discussed in §1, previous studies of SN87A have been forced to use velocities as low as  $v_a \sim 5 \text{ km s}^{-1}$  to recover the low ring expansion speed,  $v_{\varpi}$ . The hydrodynamics of Wind Compression naturally reduces  $v_a$  at the equator, since mass conservation requires that the density is inversely proportional to the velocity. The reduced wind speeds at the equator allow us to use larger, more canonical values, of the RSG wind speed.

The models with and without a disk differ most notably in the ratio  $R_o$ . Assuming that the outer rings lie at the widest point on the lobes, the observed value is  $R_o \sim 2$ . The model

with the disk has  $R_o = 4.9$ , whereas for the model without the disk,  $R_o = 2.6$ . The difference can be explained as follows: When a disk forms, its high density severely inhibits expansion of the ambient shock at the equator. A discontinuity in the shell radius  $L(\theta)$  occurs just above (below) the equator in these models. The BSG wind is able to expand rapidly along the top and bottom edges of the disk producing a strongly “wasp-waisted,” or pinched bubble. It is possible that such configurations are an artifact of our calculations. Numerical simulations have demonstrated that the lobes of energy conserving bubbles can experience considerable shaping due to non-linear effects associated with the wind shock. If the wind shock is not spherical but assumes a prolate geometry, then post-shock BSG gas is focused towards the poles (Frank & Mellema, 1996). The higher ram pressures associated with this “shock focusing” will tend to elongate the bubble, reducing  $R_o$  (BL94). Frank & Mellema (1994) found that higher values of  $p$  produce stronger shock focusing. These effects will not be seen with a self-similar method which assumes the shell is driven by an isobaric “hot bubble”. An isobaric bubble can not be produced with an aspherical wind shock.

Figs. 1 and 2 and the ring properties given in Table 1 demonstrate the success of the unified GWBB and WCD models for SN87A. This represents one of the principal conclusions of our study. We take the cases represented in Figs. 1 and 2 as our fiducial models.

### 3.2. Variation of Parameters

We have varied the five input parameters to determine (1) the effect each has on the properties of the solutions, and (2) the degree to which the input parameters constrain the solutions. In particular, we are interested in the range of  $\Omega$  necessary to match observations, given that the RSG and BSG wind parameters are within the canonical range of values (*e.g.*,  $v_a \sim 20 \text{ km s}^{-1}$ ,  $400 \lesssim v_f \lesssim 600 \text{ km s}^{-1}$ ,  $\dot{M}_a \sim 10^{-5} M_\odot \text{ yr}^{-1}$ ,  $\dot{M}_f \sim 10^{-7} M_\odot \text{ yr}^{-1}$ ). We find we can bracket the appropriate values of  $\Omega$ . Our results show that solutions outside the range  $0.3 \lesssim \Omega_c \lesssim 0.36$  do not produce reasonable results for the bubble parameters. We therefore confine our discussions to cases within that range.

$\Omega$	$v_a$	$\dot{M}_a$	$v_f$	$\dot{M}_f$	$v_{\varpi}$	$n_{\text{eq}}$	$R_o$
	km s <sup>-1</sup>	10 <sup>-5</sup> M <sub>⊙</sub> yr <sup>-1</sup>	km s <sup>-1</sup>	10 <sup>-7</sup> M <sub>⊙</sub> yr <sup>-1</sup>	km s <sup>-1</sup>	cm <sup>-3</sup>	
Fiducial Model 1 : Wind Compressed Zone							
0.3	20	2	400	1	8.30	0.87	2.6
Fiducial Model 1 : Wind Compressed Disk							
0.36	20	1	600	3	8.36	7.0	4.9
variation of parameters:							
0.33	20	2	400	1	7.02	1.9	3.2
0.3	25	2	400	1	8.23	0.73	2.7
0.3	20	1	400	1	10.5	0.47	2.5
0.3	20	2	600	1	10.7	0.94	2.4
0.3	20	2	400	3	11.7	0.97	2.4

Table 1: Dependence of the properties of the models (inner ring expansion speed  $v_{\varpi}$ , inner ring number density  $n_{\varpi}$ , and ratio of width of outer to inner rings,  $R_o$ ) on the input parameters ( $\Omega$  ratio of RSG rotation rate to breakup rotation rate, RSG wind speed  $v_a$  and mass loss rate  $\dot{M}_a$ , BSG wind speed  $v_f$  and mass loss rate  $\dot{M}_f$ ).

As mentioned above, we find two models which provide agreement with the observed ring expansion speed: one with a disk, and one without. As  $\Omega$  increases, so does the pole-to-equator density contrast (and thus  $R_o$ ). This results in higher equatorial densities, and thus smaller central ring expansion speeds. For a critical value of  $\Omega = \Omega_c$  such that  $0.3 \lesssim \Omega_c \lesssim 0.36$ , the wind asymmetry function develops a discontinuity with respect to  $\theta$ , representing the presence of a disk. Models with a disk have considerably higher equatorial density, and must have correspondingly higher values of the BSG speed and mass loss rate if the same ring expansion speed is to be obtained (see Table 1).

Increasing  $v_f$  or  $\dot{M}_f$  results in a greater BSG wind momentum flux. This causes the central ring to expand at a higher rate, so  $v_{\varpi}$  is higher. This enables the bubble to sweep up more of the

RSG wind per unit time, resulting in a larger central ring density.

Models with a higher value of  $v_a$  possess a weaker RSG shock, resulting in lower equatorial expansion speeds and lower equatorial densities. When the RSG mass loss rate is decreased,  $v_\infty$  increases, due to the smaller inertia of the RSG wind. Also, a smaller  $\dot{M}_a$  means less mass is swept-up by the expanding bubble; thus, the ring density is lower.

Table 1 shows that the combined WBB/WCD model can be strongly constrained by input parameters and observations.

#### 4. Binary Merger Model

As was seen in the previous section, for reasonable wind speeds and mass-loss rates, the RSG must have been rotating at least at  $\sim 0.3$  of the breakup rotation rate. This is higher than can be expected for a single star (Fukuda, 1982; *cf.* Heger & Langer, 1998). Thus, our results imply the presence of a binary companion in order to spin-up the primary (Soker, 1998). In this section we present a simple model for a binary merger, and find the companion mass needed to achieve the rotation rates found in §3.2. Since we assume the companion to be of a much lower mass than the primary, it is expected that once the primary fills its Roche lobe, a dynamical mass transfer process will ensue (*e.g.*, Rasio & Livio, 1996) with the subsequent spiraling-in of the companion, inside the common envelope.

In order to obtain a simple lower limit estimate for the ratio of the mass of the companion to the mass of the primary,  $q \equiv M_p/M_c$ , we assume that in the process of coalescence, the companion mass is added to the core of the primary, while all of its angular momentum serves to spin-up the primary’s envelope (see Fig. 4). The initial angular momentum of the system is given by

$$l_i = \left[ \frac{G(M_p M_c)^2}{M_p + M_c} a \right]^{1/2}, \quad (36)$$

where  $a$  is the distance between the center of masses of the primary and companion. Given that the angular momentum after coalescence is primarily that of the envelope, the final angular

momentum is

$$l_f = \xi M_e R_e^2 \Omega_r, \quad (37)$$

where  $\Omega_r \equiv \Omega \Omega_K$  is the rotation rate (and  $\Omega_K$  the breakup rotation rate),  $\xi$  is the square of the gyration radius,  $R_e$  is the radius, and  $M_e = M_{e0} = M_{e1}$  is the envelope mass, which is assumed to remain the same during coalescence. Setting  $l_i = l_f$  and simplifying, we find

$$M_e^{-1} M_c M_p (M_p + M_c)^{-1/2} (M_e + M_{c1})^{-1/2} = \xi \left( \frac{R_e}{a} \right)^{1/2} \Omega. \quad (38)$$

We assume that the final radius is approximately equal to the “volume equivalent” radius of the Roche lobe of the primary,  $R_V = a \tilde{R}_V(q)$ , where  $\tilde{R}_V$  may be approximated by the function

$$\tilde{R}_V = \frac{0.49q^{2/3}}{0.6q^{2/3} + \ln(1 + q^{1/3})} \quad (39)$$

(Eggleton, 1983), valid for all  $q$ . Using the assumption that  $M_c \ll M_p$ , equation (38) may be further simplified, as

$$(1 + q)^{-1} \approx \xi \tilde{R}_V^{1/2}(q) \Omega. \quad (40)$$

If we assume that the total mass is given by  $M_c + M_p = 20M_\odot$  [so that  $q = M_p/M_c = (20M_\odot - M_c)/M_c = 20/M_c - 1$ ] (Podsiadlowski, 1992), we may solve for the lower limit on the companion mass:

$$M_c \approx 20M_\odot \xi \Omega \tilde{R}_V(q). \quad (41)$$

For a giant star,  $\xi \approx 0.1$  (*e.g.*, Pringle 1974). Equation 41 is a nonlinear equation for  $M_c$  which may be solved numerically. For these values of  $(M_c + M_p)$  and  $\xi$  and for  $\Omega \lesssim 0.5$ ,  $\tilde{R}_V$  is close enough to constant that  $M_c$  is approximately given by the linear function  $M_c \approx 1.6\Omega$ . As a result, for  $\Omega = 0.3$ , the minimum companion mass is  $\sim 0.5 M_\odot$ . For the model with a disk, the minimum companion mass is predicted to be slightly higher,  $M_c \approx 0.6 M_\odot$ .

We must also consider the fact that material may also be ejected in the CE phase solely because of the the transfer of orbital energy into the envelope. As others have noted this is indeed a second possible mechanism for the development of the ring. The difficulty with using

such a scenario to link the shape of the nebula with the progenitor is that no simple way exists to connect the properties of the binary with the shape of the ejected slow wind and hence with the eventual shape of the bipolar nebula. Calculation of the ejection process requires expensive 3-D calculations and these only provide information about relatively small scales ( $R < 10^{14}$  cm, Sanquist *et al.* 1998). Thus while envelope ejection is alternative possibility which should be explored the advantage of the WCD model is that one can make definite statements about its consequences for the nebula via purely analytical methods.

The dividing line between the WCD and envelope ejection models is determined by  $\alpha_{CE}$ , the ratio of the envelope binding energy to the binary orbital energy which can be expressed as (de Kool 1990);

$$\alpha_{CE} = \frac{E_{env}}{\Delta E_{orb}} = \frac{4a_f M_p M_c}{a_i M_c M_e - a_f M_p M_c} \quad (42)$$

where  $a_i$  and  $a_f$  are the initial and final orbital separations. If  $\alpha_{CE} > 1$  then the entire envelope will not be lost in the CE phase. Consideration of this equation for parameters used in our models shows that if much of the orbital energy is deposited at radii  $> .01R_e$  then  $\alpha_{CE} > 1$  and we can expect the WCD to create a equatorial disk. It is possible that some mass is ejected in the early stages of the CE before the WCD begins. In fact, Soker (1998) recently proposed such a model to explain the presence of the two outer rings.

We note also Podsiadlowski's (1992) suggestion that a binary merger is responsible for the transition from the RSG to BSG. While our model is independent of the Podsiadlowski scenario it useful to compare the time scale for the two processes. Podsiadlowski quotes time scales for the merger process of a few  $10^3$  years. An upper limit on the time scale for the life of WCD is given simply by the dynamical time scale for the equatorial slow wind material,

$$\tau_{WCD} \leq \tau_{dyn} = \frac{R_{ring}}{V_a} \frac{10^{17} \text{ cm}}{5 \text{ km s}^{-1}} \approx 10^4 \quad (43)$$

The dense torus resulting from the WCD does not, however, have to be as large as the ring is

currently. It could have had a much smaller spatial extent ( $R \approx 10^{16}$ ) and still produce a nebula of the right size. Dwarkadas & Balick (1998), have shown that even a very small ( $R \approx 10^{14}$ ) dense ring can hydrodynamically shape a bipolar nebula. Thus the time scales needed to create the BSG and the WCD appear close.

We note also from Iben & Livio (1993) that  $\gamma_{CE}$ , the ratio of the spin up time scale to the orbital decay time scale has the following proportionality

$$\gamma_{CE} = \frac{\tau_{spin}}{\tau_{decay}} \propto \frac{\hat{\rho}}{\bar{\rho}}, \quad (44)$$

where  $\hat{\rho}$  is the local density the secondary star experiences as it spirals inward and  $\bar{\rho}$  is the (considerably larger) average density for the RSG. Thus for an extended star like a RSG,  $\gamma_{CE} < 1$ , and the envelope will be quickly spun up allowing the WCD mechanism to operate.

## 5. Discussion and Conclusions

We have developed a model for the bipolar nebula surrounding Supernova 1987A. As in previous investigations, we invoke the interaction between a fast isotropic Blue Supergiant Wind (BSG) and a slow aspherical (toroidal) Red Supergiant Wind. The novel aspect of our model is the use of the Wind Compressed Disk (WCD) model to determine the geometrical properties of the RSG wind. Wind compression occurs when a star rotates fast enough to deflect wind streamlines towards the equator. The increased density and reduced velocity in the equatorial-zone RSG wind provides the constraint which shapes the final wind blown bubble (WBB). The degree of wind compression depends on the characteristics of the star. Thus our model allows the observable nebular properties to be directly linked to the unobservable properties of SN87A’s progenitor.

Our results show that the combined WCD/WBB model can recover the observed size, speed, density and gross morphology of SN87A’s circumstellar nebula. Wind compression allows our models to recover the low expansion speeds of the ring without resorting to anomalously low values of the RSG wind speed. In addition, we have shown that our models are sensitive to initial

conditions allowing us to bracket the properties of the progenitor. In particular our models predict that the rotation rate of the progenitor must have been a significant fraction of the critical speed for break-up,  $\Omega \gtrsim 0.3\Omega_K$ . Since this is too large to be expected for a single RSG we infer that SN87A’s progenitor was probably spun-up by a companion. Since no companion is visible now, we have developed a simple model for a binary merger. This model, along with the results of the WCD/WBB calculations, allows us to predict that SN87A had a companion with a mass of  $M_c \gtrsim 0.5 M_\odot$ .

Our value for  $M_c$  clearly represents a lower limit. In addition to the fact that we have assumed an angular momentum deposition with 100% efficiency into the envelope, other effects also need to be considered. The shape of the bubble and speed of the ring are determined by the density contrast in the RSG wind. The formulation of the WCD model relies on an approximate method for tracing RSG wind streamlines. This ignores pressure effects. At large distances from the star it is likely that the wind compressed disk zone would experience some re-expansion which would weaken the density contrast. It is noteworthy that Garcia-Segura, Langer & MacLow (1997a) in their numerical WCD/WBB models for  $\eta$  Carina found extreme stellar rotation rates  $\Omega \sim 0.9\Omega_K$  were required to recover the correct morphology. The rapid evolution and high stellar temperature  $T_*$  associated with  $\eta$  Car make it quite different from SN87A. However the Garcia-Segura models indicate that time-dependent hydrodynamic effects may change the properties of the disk. Thus, for SN87A, we expect larger values of  $\Omega$  would be required to produce high values of  $p$  and the correct inner-ring expansion speed. As equation (41) demonstrates, larger values of  $\Omega$  imply higher companion masses.

In addition, we should note that the coalescence process is likely to produce some mass-loss which was not included in the calculation. A more accurate estimate of  $M_c$  will therefore require both a complete common envelope evolution calculation as well as the use of numerical simulations of the bubble evolution.

In spite of these uncertainties, our models provide a link between the properties of the circumstellar nebula and the progenitor star. Our results strongly indicate that SN1978A had a

binary companion which merged with the primary before the supernova explosion. A companion with a mass  $M_c \sim 3 - 6M_\odot$  (as suggested by stellar evolution calculations; *e.g.*, Podsiadlowski 1992) is perfectly consistent with the dynamical considerations in the present work.

We would like to thank Arlin Crotts, Larry Helfer and Peter Lundqvist for helpful discussions. Support for AF and TC was provided at the University of Rochester by NSF grant AST-9702484 and the Laboratory for Laser Energetics. ML acknowledges support from NASA Grant NAG5-6857.

## REFERENCES

- Balick, B. 1987, AJ, 94, 671
- Blondin, J., & Lundqvist, P, 1993, ApJ, 405, 337 (BL93)
- Burrows, C. *et al.* 1995, ApJ, 452, 680
- Bjorkman, J. E., Cassinelli, J. P. 1993, ApJ, 409, 429 (BC)
- Brander, W, Chu, Y, Eisenhauer, F, Grebel, E., Points, S.1997, ApJ, 489, 153
- Crotts, A., Kunkle, W., & Heathcote, S., 1995, ApJ, 438, 724
- Crotts, A, 1998, in press
- de Kool, M., 1990 ApJ, 358, 189
- Dwarkadas, V. V., Chevalier, R. A., Blondin, J. M. 1996, ApJ, 457, 773
- Dwarkadas, V., & Balick, B., 1998, ApJ, submitted
- Eggleton, P. P. 1983, ApJ, 268, 368
- Frank, A., Balick, B., Icke, V., & Mellema, G., 1993, ApJ, 404, L25
- Frank, A., & Mellema, G., 1994b, ApJ, 430, 800
- Frank, A., Balick, B., & Davidson K., 1994, ApJ, 441L, 77
- Frank, A., & Mellema, G.,1997, MNRAS, 292, 795
- Frank, A., 1998, New Astronomy Reviews, in press
- Fukuda, I., 1982, PASP,94, 271
- Garcia-Segura, G., Langer, N., & Mac Low, M., 1997a, in *Luminous Blue Variables: Massive Stars in Transition*, ed A. Nota & J.G.L.M. Lamers (ASP Conference Series, San Francisco)
- Garcia-Segura, G., Langer, N., Rozyczka, M., Franco, J., & Mac Low, M., 1997b, in *The Sixth Texas-Mexico Conference on Astrophysics: Astrophysical Plasmas Near and Far*, Rev Mex AA, eds. S. Torres-Peimbert & R. Dufour

- Garcia-Segura, G., Langer, N., Rozyczka, M., Franco, J., & Mac Low, M., 1997a, in *The Sixth Texas-Mexico Conference on Astrophysics: Astrophysical Plasmas Near and Far*, Rev Mex AA, eds. S. Torres-Peimbert
- Garcia-Segura, G., Mac Low, M., Langer, N., 1996, A&A, 305, 229
- Giuliani, J. L. 1982, ApJ, 256, 624
- Habing, H., 1996, A&AR, 7, 97
- Henney, W.J., & Dyson, J.E., 1992, A&A, 261, 301
- Heger, A., & Langer, N., 1998, A&A, in press
- Iben, I. & Livio, M., 1993, PASP, 105, 1373
- Ignace, R., Cassinelli, J. P., & Bjorkman, J. E. 1996, ApJ, 459, 671 (ICB)
- Koo, B.C., & McKee, C.F., 1992, ApJ, 388, 93.
- Kahn, F. D., & West, K. A., 1985, MNRAS, 212, 837
- Lundqvist, P., Sonneborn, G. 1997, in *SN 1987A: Ten Years After*, eds. M. Phillips and N. Suntzeff
- Livio, M., & Soker N., 1988, ApJ, 329, 764
- Livio, M., 1998, in *Planetary Nebulae, Proceedings of IAU Symp. # 180*, ed H. J. Habing & H.J.L.M. Lamers (Kluwer, Dordrecht), pg. 74
- Livio, M., 1997, SSR, 82, 389
- Lloyd, H.M., O'Brian, T.J., & Kahn, F., 1995, MNRAS, 273, L19
- Luo, D., & McCray, R., 1991, ApJ, 379, 659
- Meyer, F., 1997, MNRAS, 285, L11
- Meaburn, J., Bryce, M., Holloway, A. J. 1995, A&A,
- Martin, C. L., & Arnett, D, 1995, ApJ, 447, 378 (MA95)
- McCray, R., Lin, D. N. C 1994, Nature, 369, 378

- Manchado, A, Guerrero, M., Stanghelli, L., & Serra-Ricart, M., 1996 "The IAC Catalog of Northern Galactic PNe", (IAC, La Laguna)
- Nota, A., Livio, M., Clampin, M., & Schulte-Ladbeck, R., 1995, ApJ, 448, 788-299, L1
- Owocki, S. P., Cranmer, S. R., & Blondin, J. M. 1994, ApJ, 424, 887
- Podsiadlowski, P, 1992, PASP, 104, 717
- Podsiadlowski, P, Fabian, A.C., & Stevens, I.R., 1991, Nature 354, 43
- Pringle, J.E., 1974, MNRAS, 168, 137
- Rasio, F., Livio, M., 1996, ApJ, 471, 366
- Schwartz, H. E., Corradi, R. L. M., Melnick, J. 1993, A&A, 268, 714
- Soker, N., & Livio, M., 1989, ApJ, 339, 268
- Soker, N., 1998, ApJ, 496, 833
- Soker, N., 1998, submitted
- Sanquist, E., Taam, R., Chen, X., Bodenheimer, P., Burkert, A., 1998, ApJ, 500, 909
- Terman J. L., Taam, R.E., & Hernquist, L., 1995, ApJ, 445, 367
- Wang, L., & Mazzali, P., 1992, Nature, 355, 58
- Waters, L. B. F. M., Taylor, A. R., van den Heuvel, E. P. J., Habets, G. M. H. J., & Persi, P. 1988, A&A, 198, 200
- Wood, K., Bjorkman, K. S., & Bjorkman, J. E. 1997, ApJ, 477, 926
- Zickgraf, F.-J., Humphreys, R. M., Lamers, H. J. G. L. M., Smolinski, J., Wolf, B., Stalh, O. 1996, A&A, 315, 510

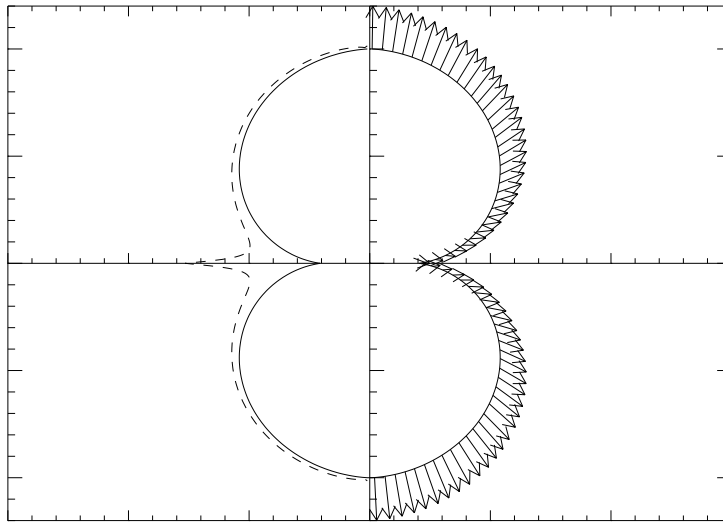


Fig. 1.— The fiducial nebula model having no disk. The radius of the solid line shows the shape of the bubble, and is proportional to its expansion speed. The arrows indicate the magnitude and direction of the flow in the shell. The distance between the dashed line and the solid line is proportional to the surface density of the bubble.

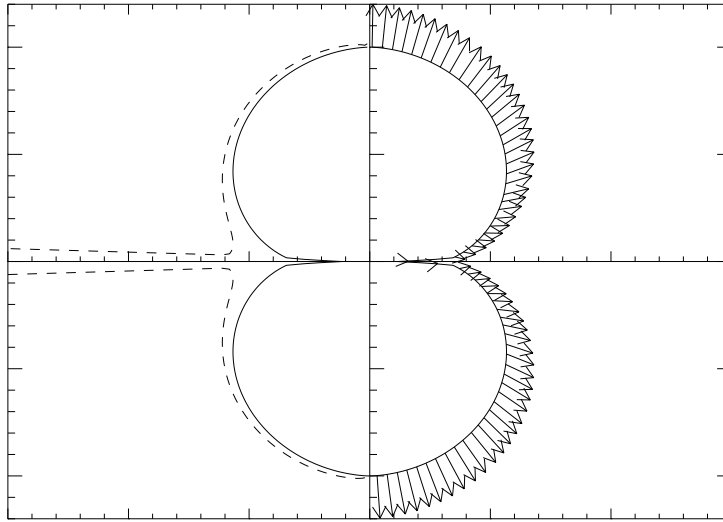


Fig. 2.— The fiducial nebula model with a disk. As in Fig. 1, the radius of the solid line shows the shape of the bubble, and is proportional to its expansion speed. The arrows indicate the magnitude and direction of the flow in the shell. The distance between the dashed line and the solid line is proportional to the surface density of the bubble. The surface density jumps drastically near the equator, indicating the presence of a dense disk.

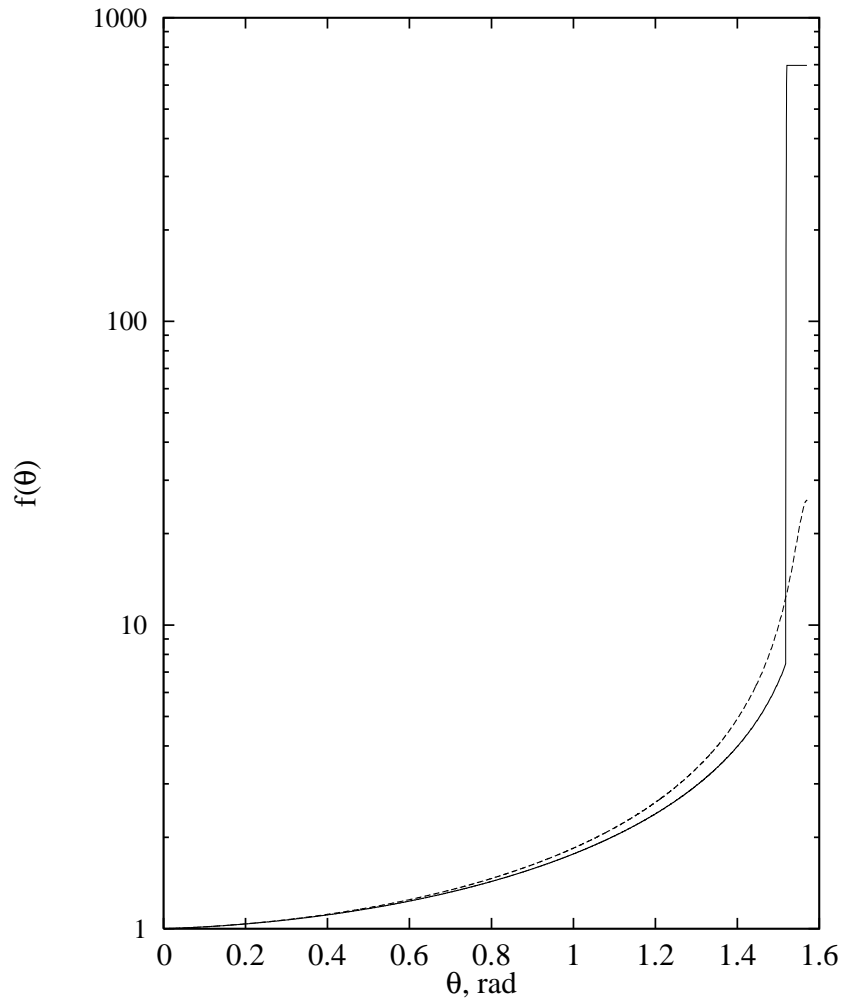


Fig. 3.— The density asymmetry functions for the RSG wind, for the models with (solid) and without (dashed) a wind-compressed disk.